Optoelectronic and thermomechanical characterization of stress-induced stability in cubic $KCdF_3$ perovskite for advanced applications

M. RIAZ[1], M. ZEESHAN[2], M. USMAN MUSHTAQ[3], M. UMER FAROOQ[2], M. SANA ULLAH SAHAR[4], M. IJAZ KHAN[2,*], ABDULLAH A. ALGETHAMI[5], HAFIZ T. ALI[5]

[1]*Institute of Physics, The Islamia University of Bahawalpur, 63100, Pakistan*
[2]*Institute of Mechanical and Manufacturing Engineering, Khwaja Fareed UEIT, Rahim Yar Khan, 64200, Pakistan.*
[3]*Department of Mechanical Engineering, KFUPM, Saudi Arabia*
[4]*Department of Mechanical, Industrial and Energy System, University of Sargodha, Sargodha - 40100, Pakistan.*
[5]*Department of Mechanical Engineering, College of Engineering, Taif University, P.O. Box 11099, Taif, Saudi Arabia*

Halide perovskites possess excellent potential for optoelectronic applications due to their unique properties. This study explores the pressure tolerance of cubic $KCdF_3$ halide perovskite. Using density functional theory (DFT) calculations, we have investigated its physical and thermodynamic characteristics under varying pressure conditions (0-100 GPa). The results have indicated its structural integrity under pressure (up to 40 GPa), accompanied by a reduction in lattice parameters. Pressure application resulted in a narrowed band gap, heightened absorption, and increased conductivity. These observations, together with high-temperature stability inferred from phonon dispersion analysis, position $KCdF_3$ as a viable contender for future optoelectronic devices.

(Received May 19, 2024; accepted October 7, 2024)

Keywords: High-pressure, Electronic structure, Optical characteristics, Thermo-mechanical properties, $KCdF_3$ perovskites properties

1. Introduction

Halide perovskites have revolutionized the landscape of optoelectronics, particularly in the realm of photovoltaics, optoelectronics, and quantum computing due to their exceptional properties. While the majority of investigations in this field have focused the conventional organic/inorganic lead-based halide perovskites, there has been a recent shift towards exploring more environmentally benign alternatives, such as lead-free and fluoride-based perovskites. Their enhanced thermal stability under varying stress conditions has recently emerged as a potential candidate in the realm of photovoltaic research [1-3]

Perovskites have the generic formula ABX_3, with A and B as cations of different sizes and X as halide anion [4,5]. More precisely, cesium lead halides emerged as highly promising luminophores, significantly enhancing laser beams, waveguides, photo-detectors, and diodes for light-emitting applications [6-8]. There are certain challenges, such as stability, which need to be addressed. Researchers have utilized various computational modeling techniques to explore the fundamental properties of perovskite and anti-perovskite materials. These techniques include density function theory (DFT) and generalized gradient approximations (GGA) [9-13]. The recently discovered wide band gap of $KCdF_3$ perovskite has several applications in diverse fields. The extensive charge recombination losses brought on by the multiple halide vacancies found in $KCdF_3$, considerably reduce the photo-detector's capacity to detect light, particularly the self-powered ones [14]. Recently, Pengjie Song et al. announced yet another significant accomplishment for the utilization of $KCdF_3$ to dope silicon-type solar material to increase their efficiency [14]. It has been shown that metal halide perovskites will transform solar energy cells and luminous diodes in astonishing ways in the future [15]. The most recent study by Aktery et al. presented DFT calculations using GGA approximations for metal halide perovskites $CsPbCl_3$. They assessed mechanical, elastic, optical, electronic, and electric properties [16]. The lattice constant, crystal lattice volume, and C_{44} elastic constant all decreased as applied pressure increased, in contrast to other metrics including electric constants, elastic moduli, Poisson ratio, and Pugh ratio. Tauc plot is used to determine the band gap energy from optical absorption spectra. From the Tauc plot of the absorbance data, Tao Lui et al. determined the optical band gaps of inorganic perovskites [16]. Long Zhang et al. then progressively placed the generated sample into a diamond anvil cell (DAC) up to 30 GPa [17], [20]. To evaluate the material's suitability for optoelectronics and related applications, the use of Ultraviolet-visible spectroscopy (UV-Vis) in combination with high-pressure techniques revealed important information about the structural and electronic characteristics of a perovskite sample under extreme conditions. Then, to get better findings, a second investigation is carried out along the same lines utilizing density functional theory (DFT) [18].

Despite extensive research on perovskites, the behavior of fluoride-based $KCdF_3$ halide perovskite under varying stress conditions remains unexplored. In light of this apparent research gap, DFT within the framework of the CASTEP code was used, to explore the potential of $KCdF_3$ halide perovskite under stress conditions (0, 20, 40, 60, 80, and 100 GPa) for technological advancement. Also, we highlight, how varying stress affects the geometrical, electronic, optical, mechanical, and thermodynamic characteristics of the designed material. Our findings provide valuable insights that may pave the way for enhanced perovskite-based devices, specifically for optoelectronic and high-temperature applications, specifically, in business, healthcare, and research, such as photo resistors [19] opto-isolators [21,22]. UV photodiodes [22,23] devices for charging linked images [22-24] as well as in photoconductive cameras [27-28] and will be helpful for experimental researchers in the future.

2. Computational details

DFT calculations, using the CASTEP algorithm under stress levels ranging from 0 to 100 GPa, were performed on a cubic unit cell with dimensions 1×1×1, containing pm-3m [221] space group [29-31]. PBE-GGA was used for the exchange-correlation functional [32-35]. The Kohn-Sham equations were used to create the computer simulations [36-38]. For the electronic structure analysis, plane wave functions as the basis set with a cutoff energy set at 330 eV, were utilized, by the ultrasoft pseudo-potential. Plane-wave functions were employed as the basis set, and a 2×2×2 Monkhorst-Pack grid was applied for Brillouin zone integration with Pulay mixing, and specific tolerances SCF set to $1x10^{-5}$ eV and $1x10^{-6}$ eV/atom, respectively. For the geometry optimization process, the BFGS (Broyden–Fletcher–Goldfarb–Shanno) algorithm was employed. It is also noted that the cubic structure distorted at 41 GPa stress.

3. Results and discussion

3.1. Geometrical properties

The unit cell structure of the designed $KCdF_3$ halide perovskite under varying stress conditions, is visualized in Fig. 1(a). As the stress increases from 0 to 100 GPa, both the lattice parameter and unit cell volume decrease, as illustrated in Fig. 1(b). The lattice parameters for $KCdF_3$ are 4.5018 Å, 4.1824 Å, 4.0281 Å, 3.9230 Å, 3.8449 Å, and 3.7813 Å, respectively, for stress values of 0, 20, 40, 60, 80, and 100 GPa corresponding to the structural properties. Our computed results are consistent with earlier work that has been published.

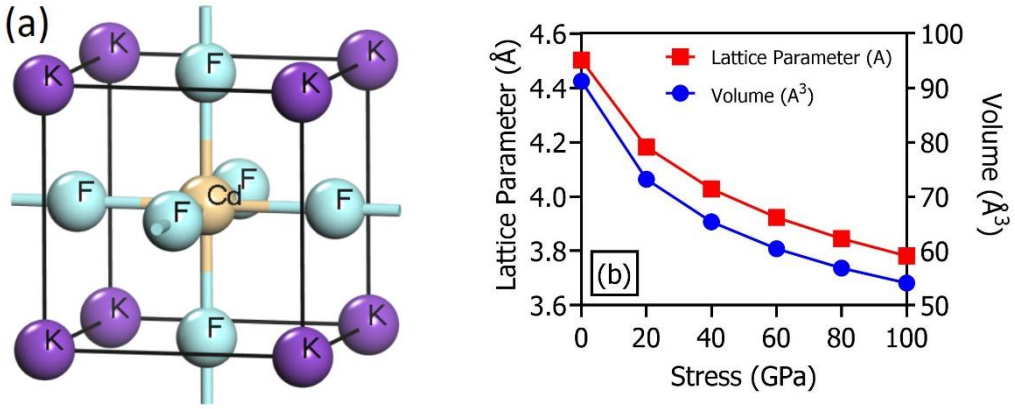

Fig. 1. (a) Supercell cubic structure of $KCdF_3$, (b) variation in the lattice parameter and volume of the unit cell as a function of stress (color online)

3.2. Electronic properties

The electronic properties of $KCdF_3$, including the band gap, TDOS, and PDOS, show that the direct band gap is minimized at the Z high-symmetry point, and the band gap decreases from 3.071 to 3.028 eV when stress rises (0, 20, 40, 60, 80, and 100 GPa), depicted in Fig. 2(a). The computed bandgap is in good agreement with those previously published [27]. The selected material displays full conductivity properties at the stress of 20 GPa and narrows as stress increases from 0 to 20 GPa, as represented in Fig. 2 (b).

From the PDOS and TDOS perspective, the band structure can be examined from multiple perspectives. From Fig. 3, it is observed that peak intensity decreases as stress level increases, expansion of the valence band occurs between 0 to –5 eV and –15 to –17 eV. While Fig. 3(c–d) distinctly shows the s and p states contribution. As seen in Fig. 3 (e), d-states significantly contribute, particularly at 0 GPa in the lower valence band area [40-42]. Fluoride s-states show prominent peaks in the –12 to –18 eV range, while p-states appear from the Fermi level to –6 eV, as shown in Fig. 3 (f–g). On the other hand, Fig. 4 displays, TDOS for Potassium (K), Cadmium (Cd), and Fluoride (F), which exhibit the significant contributions from the s and p states at 15 GPa. Based on our estimated results, the valence band properties of the K and F atomic states are enhanced, whereas the conduction band attributes of the K and Cd atomic states are slightly affected.

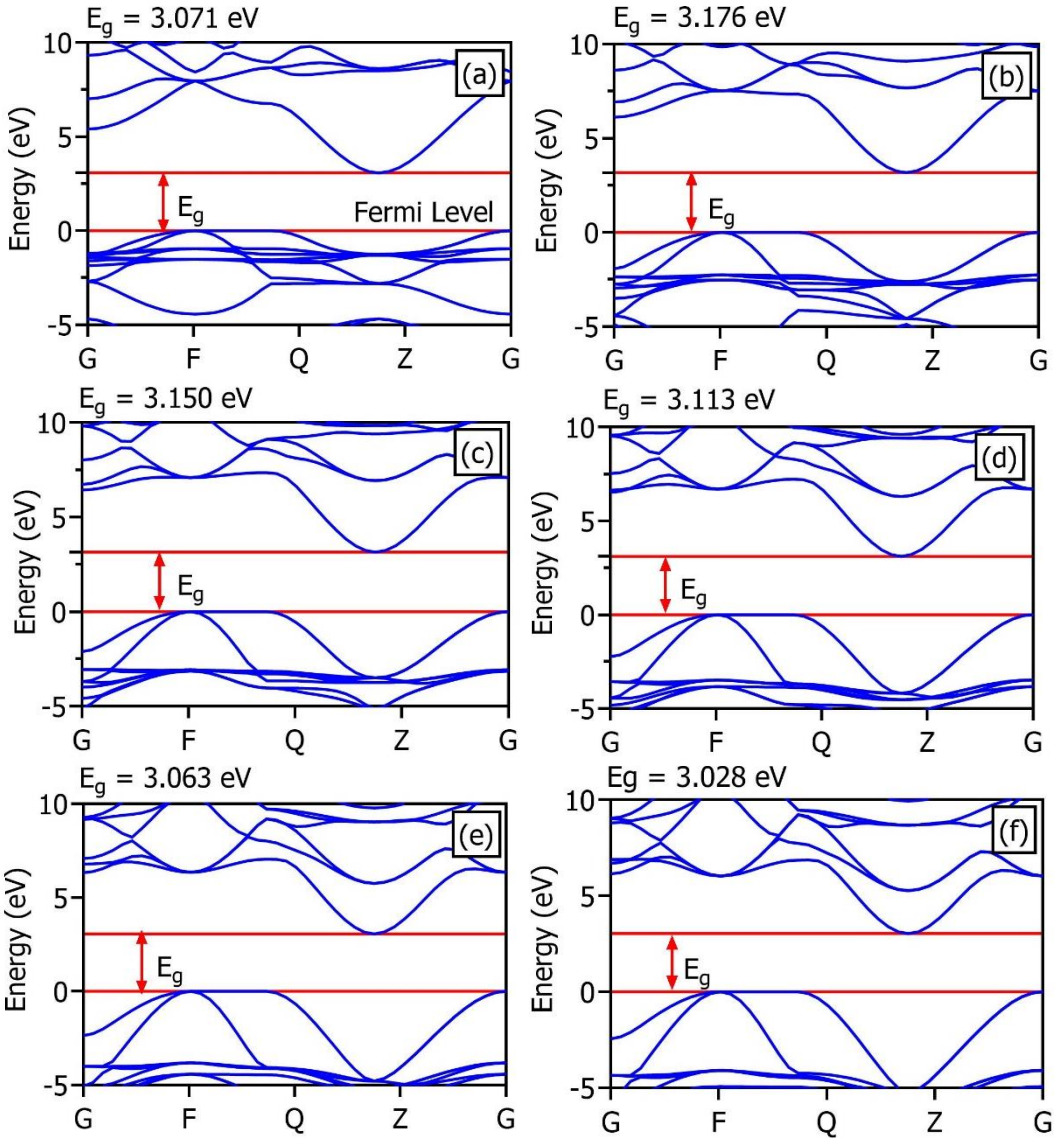

Fig. 2. Band structure of $KCdF_3$ at varying stress from 0 to 100 GPa (color online)

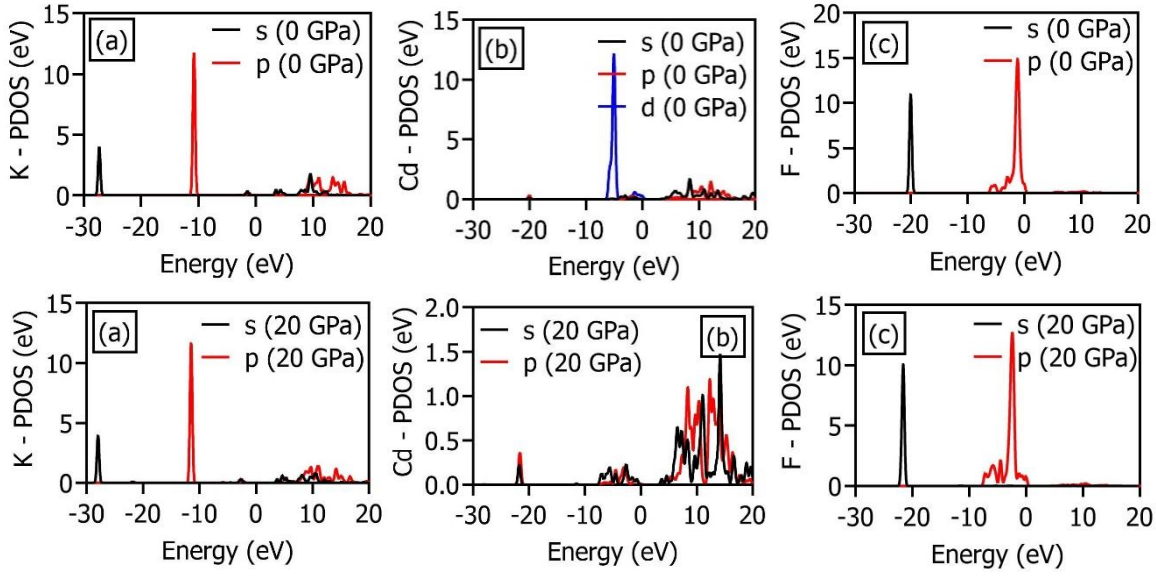

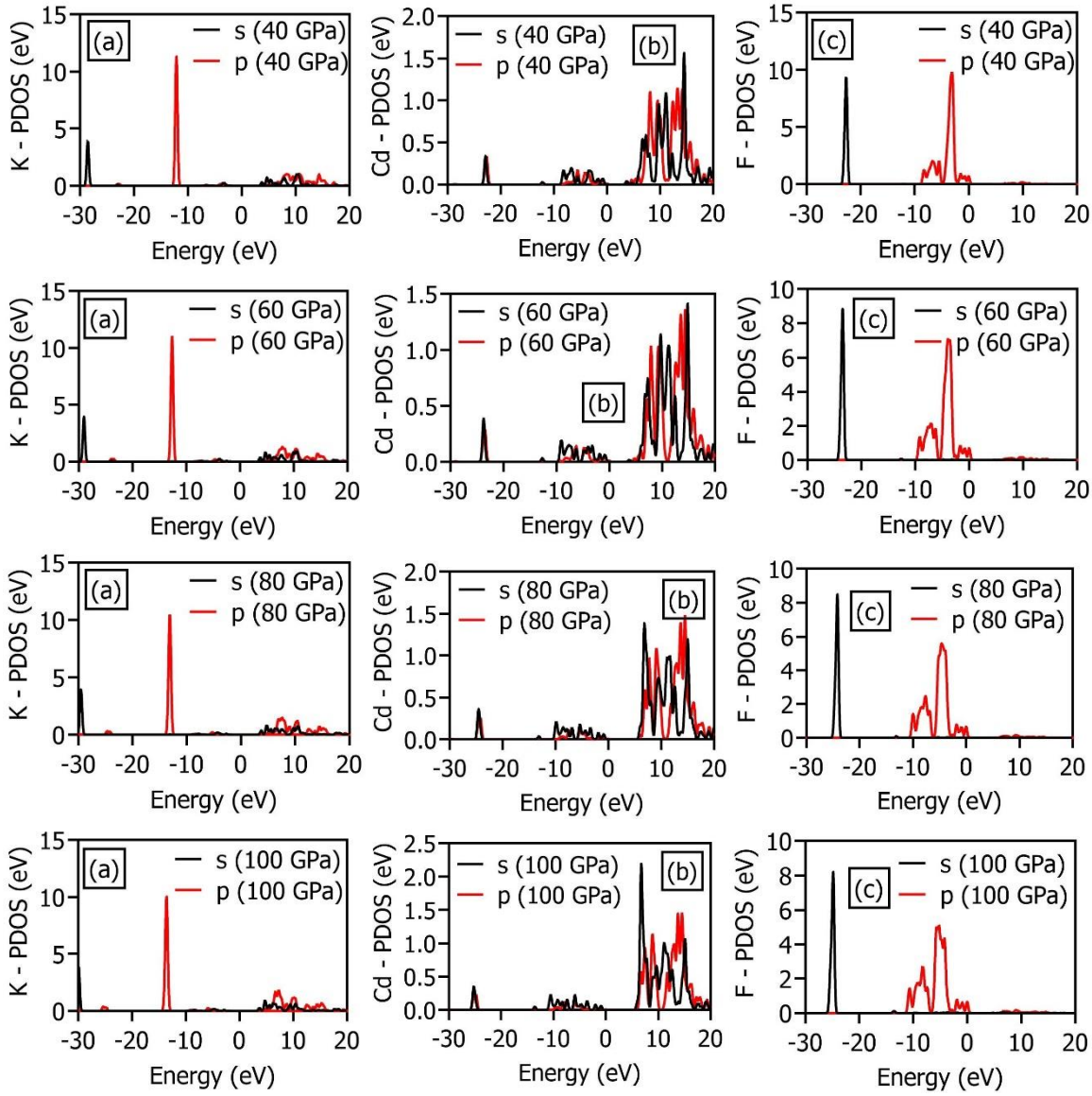

Fig. 3. Partial density of states (PDOS) of (a) K, (b) Cd, and (c) F at varying stress from 0 to 100 GPa (color online)

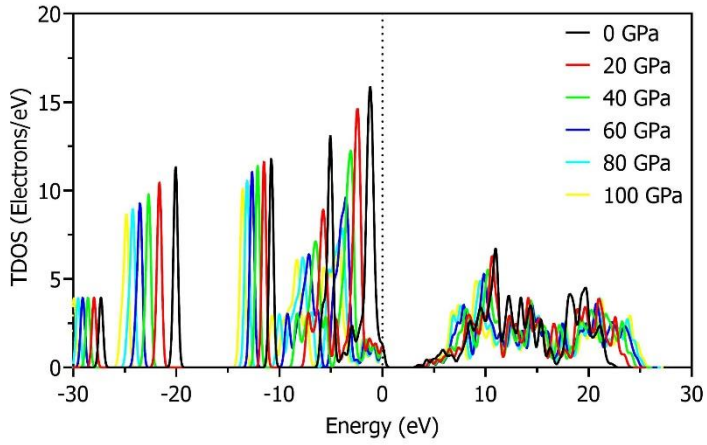

Fig. 4. Total density of states (TDOD) of $KCdF_3$ at varying stress from 0 to 100 GPa (color online)

3.3. Optical properties

Optical analysis may provide a comprehensive description of how a material interacts with the electromagnetic wave spectrum [43]. To determine the optical properties of $KCdF_3$, optical conductivity, dielectric function (both real and imaginary parts), loss function, reflectivity, and refractive index.

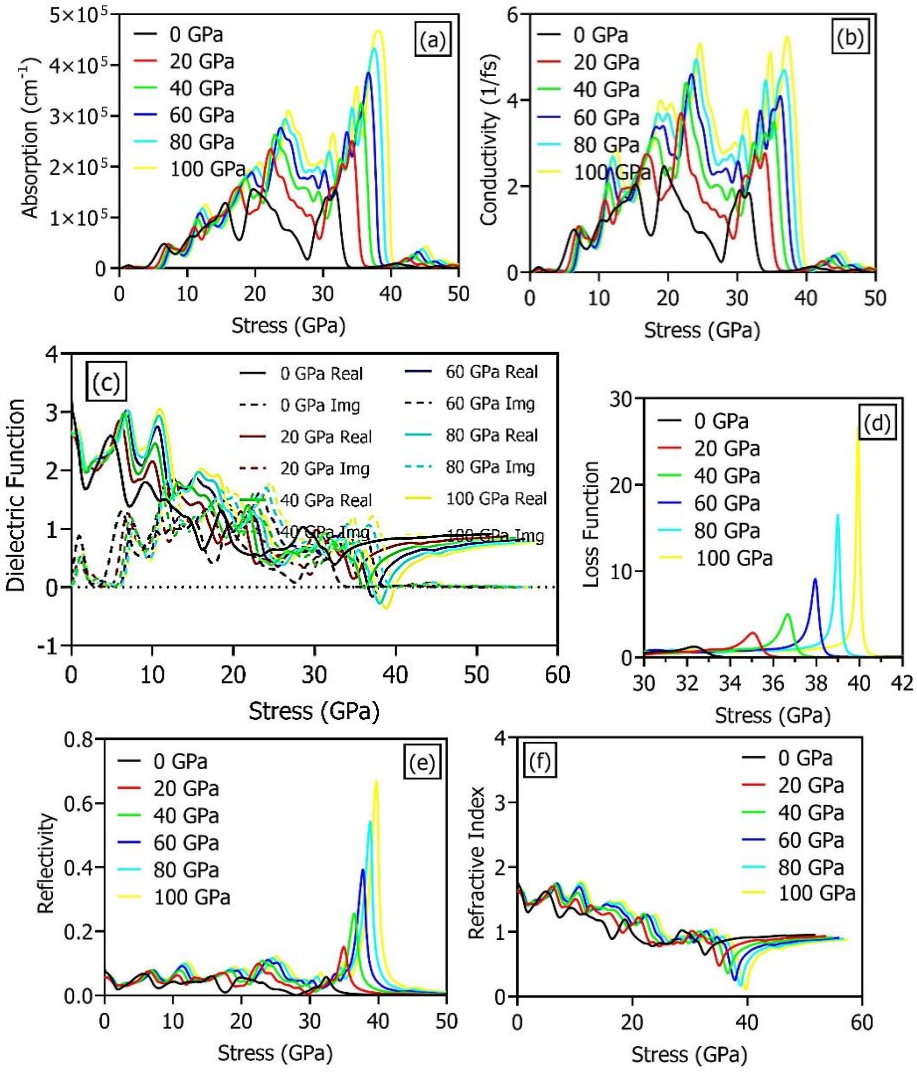

Fig. 5. (a) Absorption, (b) Conductivity, (c) Dielectric function (Real Solid Line; Img. dotted Line), (d) Loss Function (e) Reflectivity (f) Refractive index of $KCdF_3$ (color online)

The equations used for these optical properties are from the literature [44,45]. The electromagnetic absorption spectrum is predicted to be at 0, 20, 40, 60, 80, and 100 GPa. The highest absorption is found within the UV range, specifically between 5 and 40 eV, as illustrated in Fig. 5(a). From this, it can be deduced that as stress increases, the material's capacity to retain energy is also enhanced. Fig. 5(b), represents the conductivity, it is shown that stress levels affect conductivity values, when stress levels exceed 38 GPa, conductivity rises to its peak points. Fig. 5(c) depicts the dielectric behavior. It is observed that the highest peak intensity of the dielectric lies within the energy range of –0.8 to 3 eV. The energy dissipated within the medium corresponds to the imaginary component of the dielectric. Additionally, the loss function and reflectivity found direct variation with applied stress, as stress increases, both increase as shown in Fig. 5(d). Also, Fig. 5(e) shows that increased stress leads to higher reflectivity, indicating more incident light is reflected. The imaginary component of dielectric, determines the amount of light absorbed, while the real part, denotes the speed at which light travels through the material. Fig. 5(f), shows that the refractive index varies between 1.8 and 0.2.

3.4. Electron energy loss spectroscopy (EELS)

EELS analysis of potassium, cadmium, and fluoride in $KCdF_3$ under 0 to 100 GPa stress provides key insights into phase transitions, defects, electronic structure, and local bonding [1], as depicted in Fig. 6(a–f). Fig. 6(a–c) disclosed the relationship between absorption and rising energy levels, prospectively driven by the electronic configurations

and orbital transitions of the constituent atoms [47]. K atoms peak at 18 eV, Cd atoms at 20 eV, and F atoms at 10 eV, reflecting their distinct electronic structures and bonding characteristics. Fig. 6(d–f) exhibits distinct emission spectra: K atoms peak at –10 eV, Cd atoms at –50 eV, and F atoms near 0 eV. These emissions, driven by electron relaxation and atomic properties, provide insight into interaction dynamics and electron behavior.

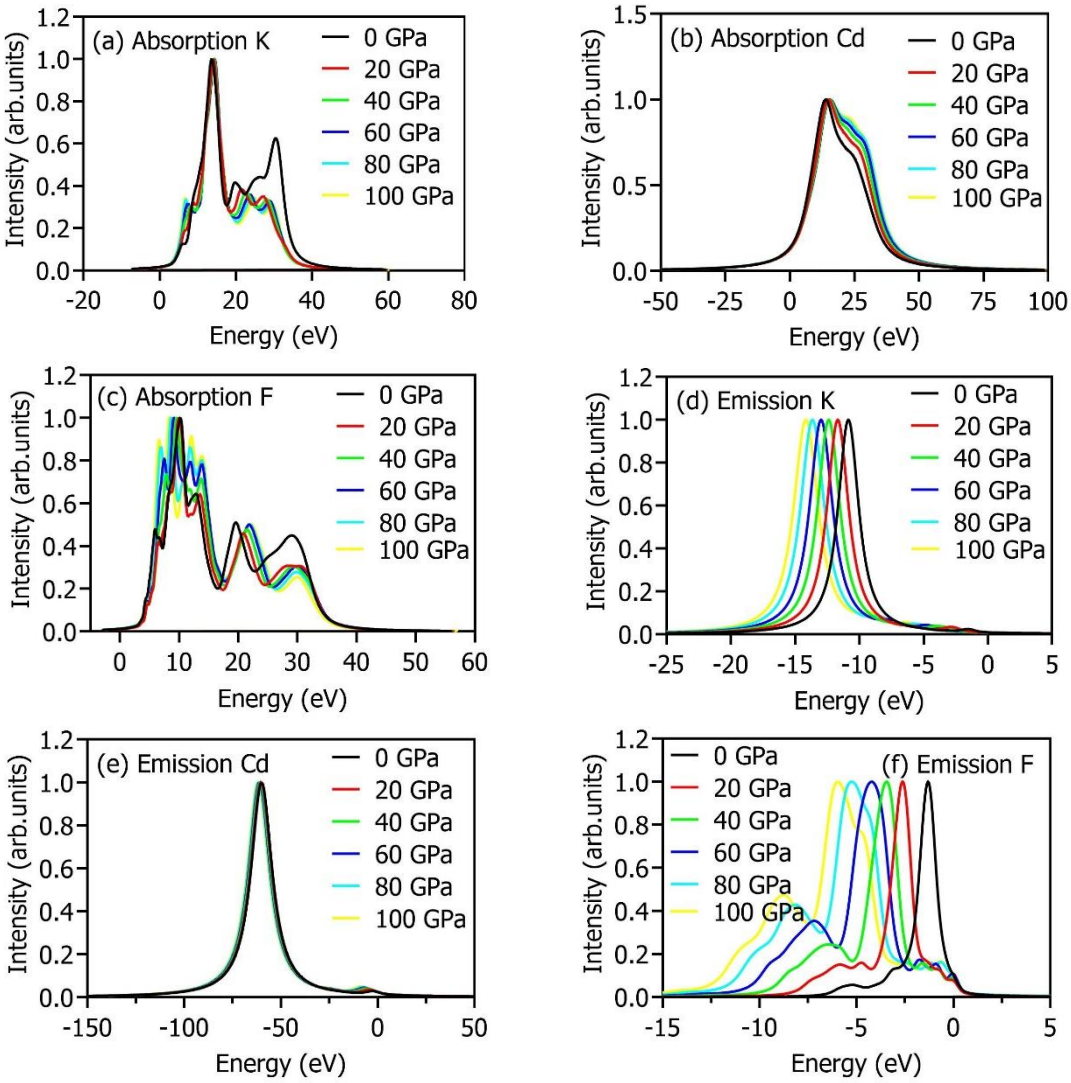

Fig. 6. Absorption of (a) Cd (b) K and (c) F and Emission of (d) K (e) Cd and (f) F at varying stress from 0 to 100 GPa (color online)

3.5. Elastic and mechanical properties

By determining the elastic constants (C_{11}, C_{12}, C_{44}), one can delve into the fundamental properties [48,49]. All these constants meet the Born stability conditions $C_{11} - C_{12} > 0$, $C_{11} + 2C_{12} > 0$, and $C_{44} > 0$. Fig. 7, presents their trend over the entire stress level, which implies the mechanical stability of the investigated compound [44].

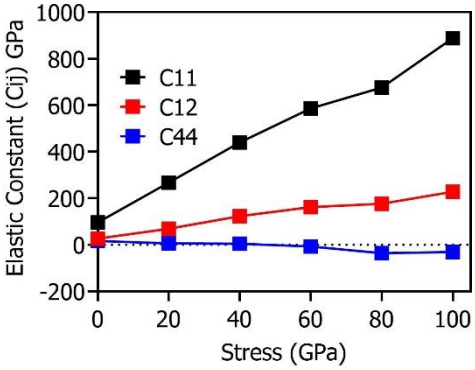

Fig. 7. Elastic constants C_{11}, C_{12} and C_{44} at varying stress from 0 to 100 GPa (color online)

Other derived parameters from elastic constants, were computed by employing the literature relation [44,45,50]. The computed values of all these derived parameters are plotted in Fig. 8. In Fig. 8(a), as the applied stress ranges from 0 to 100 GPa, B increases. Meanwhile, G) and E remain consistent with slight variations but show a noticeable decrement at 80 GPa. Fig. 8(b) predicted that the Pugh ratio (B/G) and Frantsevish ratio (G/B) have an inverse variation to each other, showing ductile character, because their values exceed their critical values [51,52]. Fig. 8(c), presents the Cauchy pressure (P_C) as a distinguishing factor between ductile and brittle behaviors [53,54]. A positive P_C indicates ductility, while a negative P_C suggests brittleness [55]. Based on the findings, the designed material demonstrates ductility over the entire stress range. Poisson's ratio (ν) is also a key parameter in determining a material's brittleness or ductility. Materials with a Poisson's ratio less than 0.26 are typically brittle, while those with a ratio greater than 0.26 are generally ductile [49–50]. As shown in Fig. 8(d), $KCdF_3$ is predicted as a ductile character. Additionally, anisotropy is highlighted in the same Fig. 8(d), indicating anisotropic because computed values are deviated from unity (A = 1) [56].

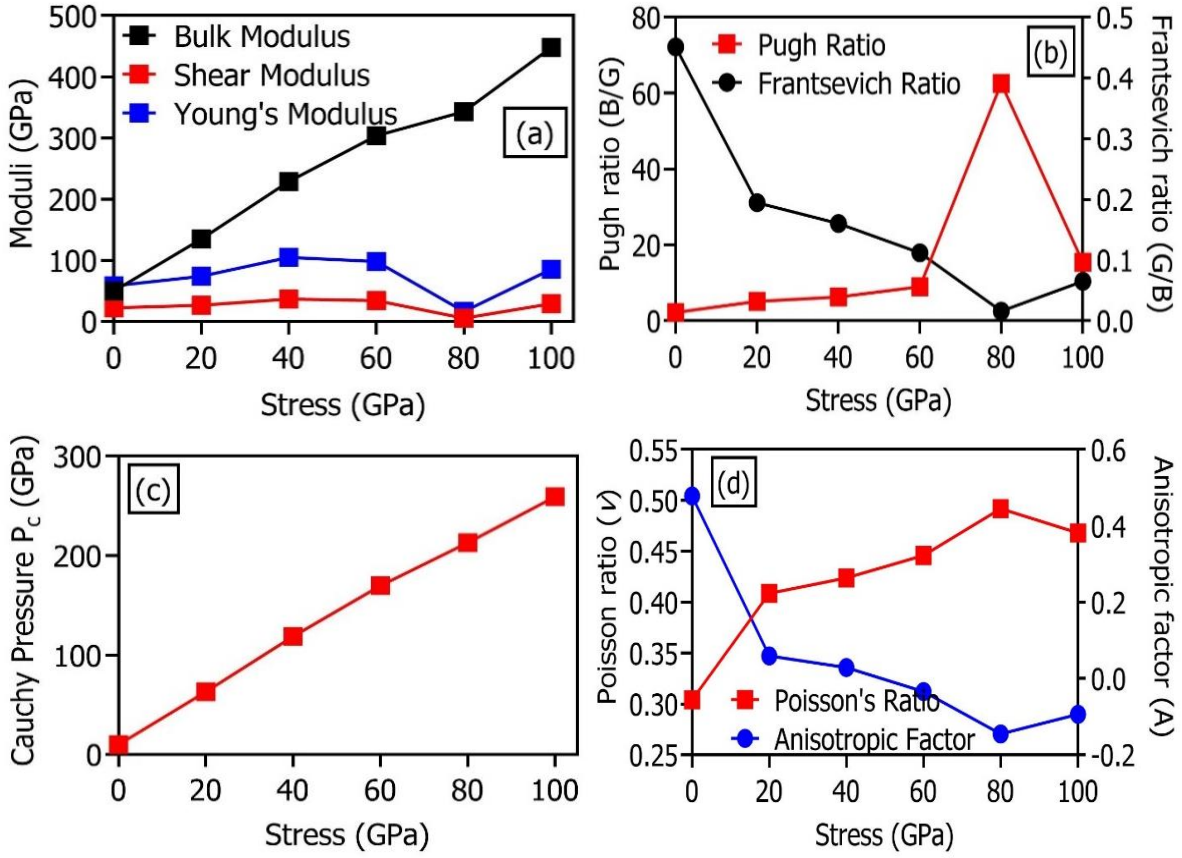

Fig. 8. (a) Elastic moduli in $KCdF_3$, (b) Frantsevich ratio, Pugh ratio (c) Cauchy Pressure (d) Poisson ratio, and anisotropic factor plotted with applied stress (color online)

3.6. Phonon dispersion and phonon DOS

The study of phonon dispersion plays a pivotal role from the perspective of the various physical, thermal, and electronic properties of materials, enabling better application, overall stability, and design of materials for specific uses [52]. Fig. 9(a–f) shows the phonon spectra of $KCdF_3$ at stress levels from 0 to 100 GPa. The increasing trend indicates that optical lattice vibrations are affected by stress from 0 to 100 GPa, confirming the dynamic stability of $KCdF_3$.

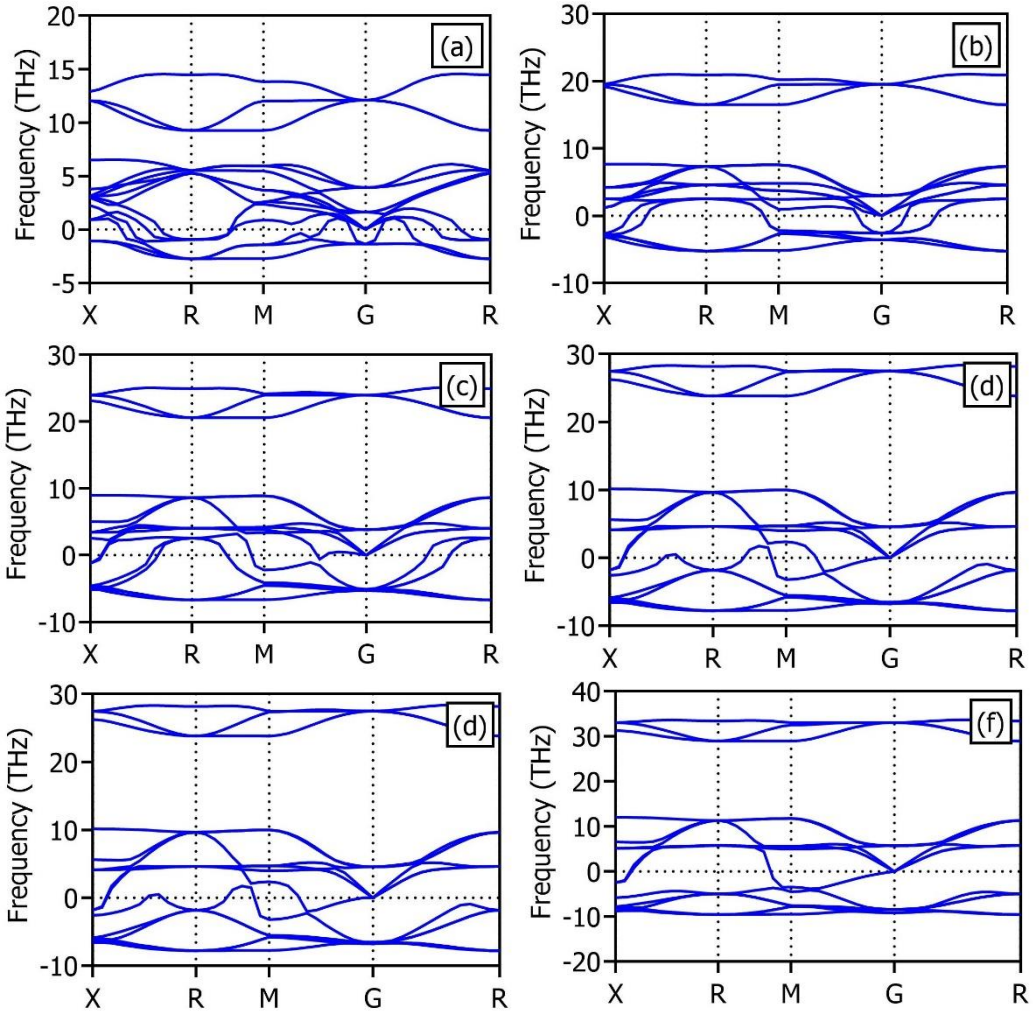

Fig. 9. Phonon dispersion at different stress values (a) 0 GPa, (b) 20 GPa, (c) 40 GPa, (d) 60 GPa, (e) 80 GPa, and (f) 100 GPa (color online)

Fig. 10 shows the phonon density of states (DOS). The density of states is derived from the phonon dispersion relation, attained vibrational modes within various frequency ranges. The Phonon Density of States (DOS) provides insights into the material's vibrational and lattice dynamics.

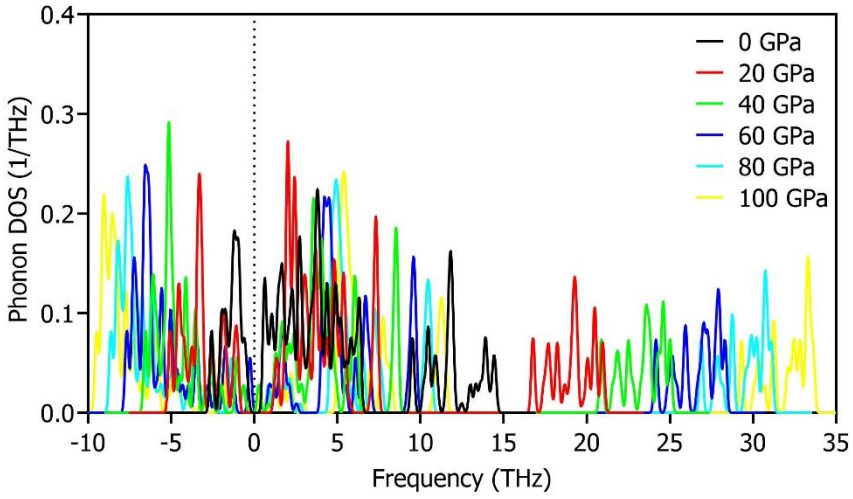

Fig. 10. Phonon DOS for $KCdF_3$ at varying stress conditions (color online)

3.7. Thermodynamic properties

Thermodynamic characteristics are fundamental for determining the system state. For $KCdF_3$, evaluation of enthalpy, free energy, entropy, heat capacity, and Debye temperature (θ_D) for $KCdF_3$ over 0 to 100 GPa and 0 to 1000 K, as depicted in Fig. 11(a–e). Fig. 11(a, c) demonstrated that enthalpy and total entropy increase linearly with applied stress. Higher stress reduces enthalpy compared to lower stress, indicating that increased stress affects molecular packing, interactions, heat capacity, phase transitions, and energy levels [57]. Fig. 11(b) shows that free energy decreases with temperature, indicating exothermic, spontaneous processes. Fig. 11(d) shows that heat capacity inversely correlates with stress from 0 to 100 GPa. Fig. 11(e) shows that the Debye temperature (θ_D) increases with temperature, indicating more intense and energetic lattice vibrations and atomic motion. Higher temperature prime to more intense atomic vibrations and enhanced stability due to increased vibrational modes.

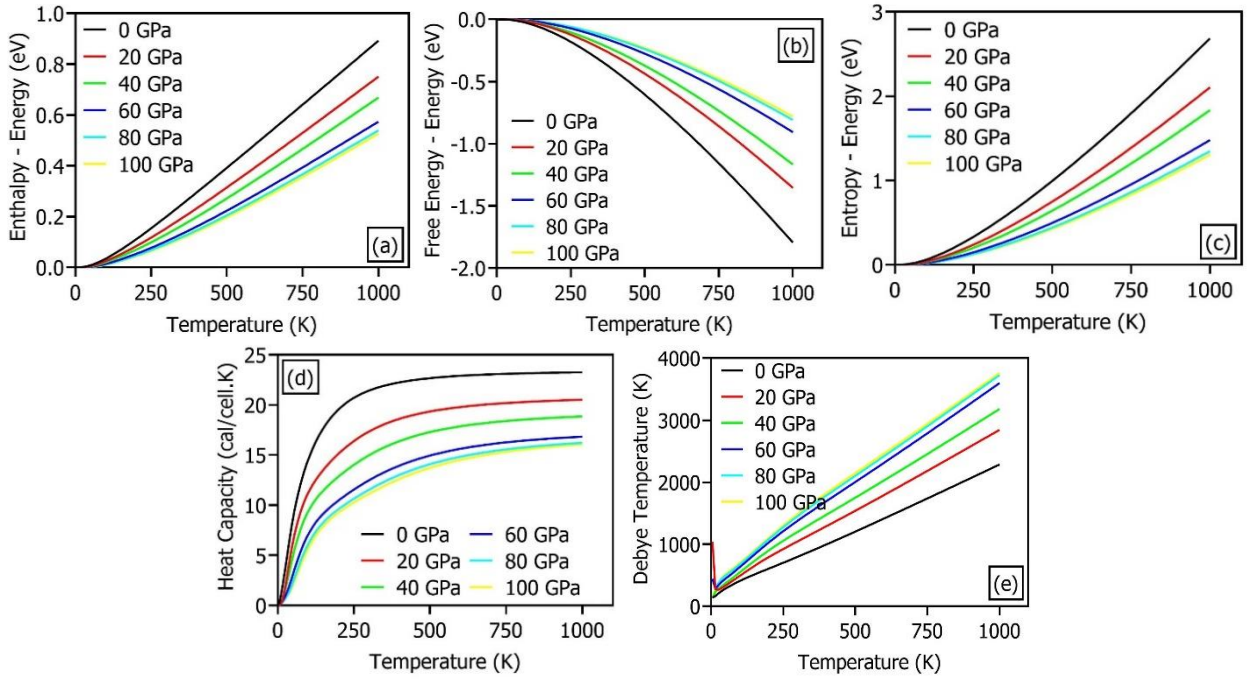

Fig. 11. (a) Enthalpy of $KCdF_3$, (b) Free energy, (c) Entropy, (d) Heat capacity, and (e) Debye temperature plotted with applied stress (color online)

4. Conclusion

DFT based on the first principal computation within the framework of CASTEP code, was performed to probe the geometrical, electronic, optical, mechanical, and thermodynamic properties of the cubic $KCdF_3$ halide perovskites under stress conditions (0, 20, 40, 60, 80, and 100 GPa), aiming for potential advanced applications. Obtained results revealed that lattice parameters, cell volume, and band gap were found to have an inverse relation with applied stress, as stress increases, these parameters decrease. The results show that the material is cubically unstable at 41 GPa and above. Optically, high absorption, high conductivity, and reflectivity were exhibited. In the case of mechanical analysis, the elastic constant satisfies the Born-stability criteria, and the derived parameter indicates the anisotropic and ductile character over the entire stress range. Further, the stability of the designed materials was also confirmed by thermodynamic properties and phonon dispersion phenomena. The designed perovskite has the potential for advanced optoelectronic and high-temperature applications, because of its high absorption, high conductivity, and large Debye temperature (θ_D), and paves the smooth path for future experimental work.

Funding

The research was funded by Taif University, Taif, Saudi Arabia (TU-DSPP-2024-285).

Acknowledgments

The authors extend their appreciation to Taif University, Saudi Arabia, for supporting this work through project number (TU-DSPP-2024-285).

References

[1] S. M. J. Zaidi, M. I. Khan, S. S. A. Gillani, M. S. U. Sahar, S. Ullah, M. Tanveer, Materials Research Express **9**(12), 125501 (2022).
[2] W. Xiang, W. Tress, Advanced Materials **31**(44),

1902851 (2019).
[3] Y. Dang, D. Ju, L. Wang, X. Tao, CrystEngComm **18**(24), 4476 (2016).
[4] U. G. Jong, C. J. Yu, Y. S. Kim, Y. H. Kye, C. H. Kim, Phys. Rev. B **98**(12), 32 (2018).
[5] S. Idrissi, H. Labrim, L. Bahmad, A. Benyoussef, Chem. Phys. Lett. **766**, 138347 (2021).
[6] J. Song, J. Li, X. Li, L. Xu, Y. Dong, H. Zeng, Advanced Materials **27**(44), 7162 (2015).
[7] S. A. Veldhuis, P/ P/ Boix, N. Yantara, M. J. Li, T. C. Sum, N. Mathews, S. G. Mhaisalkar, Advanced Materials **28**(32), 6804 (2016).
[8] L. Zhang, X. Yang, Q. Yang, P. Wang, Z. Yin, X. Zhang, H. Tan, Y. M. Yang, M. Wei, B. R. Sutherland, E. H. Sargent, J. You, Nature Communications **8**, 15640 (2017).
[9] A. A. Raiss, Y. Sbai, L. Bahmad, Journal of Magnetism and Magnetic Materials **385**, 2950 (2015).
[10] R. Khalladi, H. Labrim, S. Idrissi, S. Mtougui, I. El Housni, S. Ziti, N. El Mekkaoui, L. Bahmad, Solid State Commununications **290**, 42 (2019).
[11] Y. Selmani, M. Mouatassime, F. Goumrhar, H. Labrim, L. Bahmad, A. Benyoussef, Solid State Commununications **328**, 114254 (2021).
[12] Y. Selmani, H. Labrim, S. Ziti, L. Bahmad, Computational Condensed Matter **32**, e00699 (2022).
[13] A. Menedjhi, N. Bouarissa, S. Saib, K. Bouamama, Optik **243**, 167198 (2021).
[14] S. Cheng, X. Zheng, Z. Hou, R. Hui, S. Jiang, S. Xi, G. Wen, X. Liu, Journal of Materials Chemistry C **10**(14), 5693 (2022).
[15] A. Dumont, E. Nicholson, C. Qiu, J. Pan, Z. Gariepy, S. Du, J. Howe, C. V. Singh, Z.-H. Lu, Advanced Materials Interfaces **9**(30), 2201296 (2022).
[16] T. Liu, S. Salek, J. C. Byers, Electrochemistry Communications **143**, 107381 (2022).
[17] L. Zhang, L. Wang, K. Wang, B. Zou, Journal of Physical Chemistry C **122**(27), 15220 (2018).
[18] R. Padmavathy, A. Amudhavalli, R. Rajeswarapalanichamy, K. Iyakutti, Zeitschrift für Naturforschung A **74**(10), 905 (2019).
[19] P. Gui, Z. Chen, B. Li, F. Yao, X. Zheng, Q. Lin, G. Fang, ACS Photonics **5**(6), pp. 2113 (2018).
[20] T. Zhang, Y. Chen, Y. Chu, S. J. Ding, W. Liu, X. Wu, ACS Applied Electronic Materials **4**(6), 2805 (2022).
[21] J. Zhang, X. Yang, H. Deng, K. Qiao, U. Farooq, M. Ishaq, F. Yi, H. Liu, J. Tang, H. Song, Nano-Micro Letters **9**(3), 36 (2017).
[22] L. Yang, W. L. Tsai, C.-S. Li, B.-W. Hsu, C.-Y. Chen, C.-I. Wu, H. W. Lin, ACS Applied Materials and Interfaces, **11**(50), 47054 (2019).
[23] Q. Wang, Z. Gong, S. Wu, S. Pan, J. Pan, Journal of Crystal Growth **596**, 126838 (2022).
[24] T. Haeger, M. Ketter, J. Bahr, N. Pourdavoud, M. Runkel, R. Heiderhorr, T. Riedl, Journal of Physics Materials **3**(2), 24004 (2020).
[27] M. Bruzzi, N. Calisi, N. Enea, E. Verroi, A. Vinattieri, Frontiers in Physics **11**, 51 (2023).
[28] N. Falsini, G. Roini, A. Ristori, N. Calisi, F. Biccari, A. Vinattieri, Journal of Applied Physics **131**(1), 010902 (2022).
[29] M. Rizwan, I. Iqra, S. S. A. Gillani, I. Zeba, M. Shakil, Z. Usman, Physics of the Solid State **63**(1), 134 (2021).
[30] M. Rizwan, M. Farman, A. Akgul, Z. Usman, S. Anam, Indian Journal of Physics **96**(4), 1 (2022).
[31] L. Q. Jiang, J. K. Guo, H. B. Liu, M. Zhu, X. Zhou, P. Wu, C. H. Li, Journal of Physics and Chemistry of Solids **67**(7), 1531 (2006).
[32] G. Murtaza, Hayatullah, R. Khenata, M. N. Khalid, S. Naeem, Physica B: Condensed Matter **410**, 131 (2013).
[33] C. Dotzler, G. V. M. Williams, A. Edgar, Current Applied Physics **8**(3-4), 447 (2008).
[34] J. P. Perdew, K. Burke, M. Ernzerhof, Physical Review Letters **77**, 3865 (1996).
[35] J. P. Perdew, J. A. Chevary, S. H. Vosko, K. A. Jackson, M. R. Pederson, D. J. Singh, C. Fiolhais, Phys. Rev. B Condens. Matter **46**(11), 6671 (1992).
[36] P. Hohenberg, W. Kohn, Physical Review **136**(3B), B864 (1964).
[37] W. Kohn, L. J. Sham, Physical Review **140**(4A), A1133 (1965).
[38] W. Kohn, Reviews of Modern Physics **71**(5), 1253 (1999).
[40] V. L. Bekenev, Q. Yu. Khyzhun, A. K. Sinelnichenko, V. V. Atuchin, O. V. Parasyuk, O. M. Yurchenko, Yu. Bezmolnyy, A. V. Kityk, J. Szkutnik, S. Calus, Journal of Physics and Chemistry of Solids **72**(6), 705 (2011).
[41] O. Y. Khyzhun, V. L. Bekenev, N. M. Denysyuk, O. V. Parasyuk, A. O. Fedorchuk, Journal of Alloys and Compounds **582**, 802 (2014).
[42] T. V. Vu, A. A. Lavrentyev, B. V. Gabrelian, D. D. Vo, K. D. Pham, N. M. Denysyuk, L. I. Isaenko, A. Y. Tarasova, O. Y. Khyzhun, Optical Materials **102**, 109793 (2020).
[43] B. Luo, X. Wang, E. Tian, H. Song, G. Li, L. Li, Journal of Alloys and Compounds **708**, 187 (2017).
[44] G. Vaitheeswaran, V. Kanchana, R. S. Kumar, A. L. Cornelius, M. F. Nicol, A. Svane, N. E. Christensen, O. Eriksson, Physical Review B **81**(7), 075105 (2010).
[45] R. Hill, Proceedings of the Physical Society Section A **65**(5), 349 (1952).
[46] R. Brydson, B. G. Williams, W. Engel, H. Sauer, E. Zeitler, J. M. Thomas, Solid State Commununications **64**(4), 609 (1987).
[47] F. Hofer, F. P. Schmidt, W. Grogger, G. Kothleitner, IOP Conference Series: Materials Science and Engineering **109**(1), 8 (2016).
[48] J. Chen, X. Zhang, L. Yang, F. Wang, Communications in Theoretical Physics **73**(4), 045702 (2021).
[49] S. Ferahtia, S. Saib, N. Bouarissa, S. Benyettou, Superlattices and Microstructures **67**, 88 (2014).
[50] M. Awais, I. Zeba, S. S. A. Gillani, M. Shakil, M. Rizwan, Journal of Physics and Chemistry of

Solids **169**, 110878 (2022).
[51] M. Ahmad, G/ Rehman, L. Ali, M. Shafiq, R. Iqbal, R. Ahmad, T. Khan, S. Jalali-Asadabadi, M. Maqbool, I. Ahmad, Journal of Alloys and Compounds **705**, 828 (2017).
[52] Saad Tariq, A. Afaq, S. Saad, Samar Tariq, AIP Advances **5**(7), 77111 (2015).
[53] S. Mnasri, S. Abdi-Ben Nasrallah, N. Sfina, N. Bouarissa, M. Said, Semiconductor Science and Technology **24**(9), 1 (2009).
[54] N. Bouarissa, Optik **138**, 263 (2017).
[55] Y. Benkaddour, A. Abdelaoui, A. Yakoubi, H. Khachai, A. Al-Douri, S. Omran, A. Shankar, R. Khenata, C. Voon, D. Prakash, K. D. Verma, Journal of Superconductivity and Novel Magnetism **31**(2), 395 (2017).
[56] R. A. De Souza J. Maier, Physical Chemistry Chemical Physics **5**(4), 740 (2003).
[57] N. Bioud, K. Kassali, N. Bouarissa, Journal of Electronic Materials **46**(4), 2521 (2017).

*Corresponding author: ijazkhan4123@gmail.com